Comparison of Surface Durability & Dynamic Performance of Powder Metal & Steel Gears

A. Yoshida, Y. Ohue & Isamu Karasuno

Table I

	Pinion	Gear
Module mm	5	
Standard Pressure Angle	20°	
Number of Teeth	15	16
Addendum Modification Coefficient	+0.571	+0.560
Tip Circle Diameter mm	90.71	94.60
Center Distance mm	82.55	
Face Width mm	18	6
Contact Ratio	1.246	
Accuracy*	Class 1	Class 1
Tooth Surface Finishing	Grinding	
*JIS B 1702		

Table II

Gear Specimen		ISPM
Powder Type		0.7% Mn 1.0% Cr 0.2% Mo Balance Fe
Particle diameter μm		75–106
Mixing		0.5% Graphite 0.8% Zinc Stearate
Compacting Pressure kN/cm^2		64
Green Density g/cm^3		6.9
Sintering		1403 K x 0.5 hr N_2 Gas
Machining		Hobbing
Induction-Hardening	Frequency kHz Heating Time s	30 7.7
Tempering		453 K x 2 hr
Finishing		Grinding

Introduction

Surface-hardened, sintered powder metal gears are increasingly used in power transmissions to reduce the cost of gear production. One important problem is how to design with surface durability, given the porous nature of sintered gears. Many articles have been written about the mechanical characteristics, such as tensile and bending strength, of sintered materials, and it is well-known that the pores existing on and below their surfaces affect their characteristics (Refs. 1–3). Power transmission gears are frequently employed under conditions of high speed and high load, and tooth surfaces are in contact with each other under a sliding-rolling contact condition. Therefore it is necessary to consider not only their mechanical, but also their tribological characteristics when designing sintered gears for surface durability.

The authors have investigated the surface durability, the failure modes and the changing of contact surfaces during the fatigue process of induction-hardened, sintered powder metal spur gears and rollers (Refs. 4–7). These investigations have shown that the surface durability of induction-hardened, sintered rollers was affected by the sintered density and the powder size, and that the failure mode was spalling (Refs. 4, 7). The failure mode of the induction-hardened, sintered gears was pitting spread over the tooth surface with spalling (Ref. 5).

In this article, induction-hardened, sintered powder metal spur gears were compared with induction-hardened, melted steel spur gears for surface durability and dynamic performance using a power circulating gear testing machine. The changes in the dynamic performance and the tooth surface of both gears were measured and

observed during the fatigue processes. The differences in the surface durability and the dynamic performance between the sintered gears and the melted steel gears are discussed.

Test Gears

Induction-hardened, sintered powder metal gears (ISPM) and induction-hardened melted steel gears (ISCM) were employed as the test gears. The specifications of spur gears used in this experiment are given in Table I. These test gears had a module of 5 mm and a standard pressure angle of 20°. Case-hardened pinions (CSCM) made of chromium molybdenum alloy steel (JIS SCM415: 0.15% C) were mated with both test gears.

The manufacturing conditions of the sintered powder metal gears are given in Table II. The powder was a pre-alloyed steel. It was mixed with graphite and zinc stearate and compacted into disks having a green density of 6.9 g/cm^3. The disks were sintered, hobbed and then induction-hardened. The material of the induction-hardened, melted gears was 1.0% Cr-0.25% Mo alloy steel (JIS SCM440: 0.40% C). After hobbing, the steel gears were induction-hardened under the same conditions as the sintered gears. The tooth surfaces of both test gears were finished by grinding. The surface roughnesses along the tooth traces of gears ISPM, ISCM and CSCM were 1.6, 1.5 and 1.8 μm *Rmax*, respectively. Young's modulus and Poisson's ratio of the sintered gears were 152 GPa and 0.25. Those of the steel gears were 206 GPa and 0.3.

The hardness distributions below the tooth surfaces of the test gears and pinions are shown in Fig. 1. The hardness was measured at the working pitch point of each gear using a micro-Vickers hardness tester. The hardnesses of the tooth surfaces of test gears ISPM and ISCM were *Hv* 620 and *Hv* 700, and the total hardened depths of these test gears were 2.8 and 3.6 mm, respectively. The hardness of test gear ISPM was lower than that of ISCM in spite of the same induction-hardening conditions, since ISPM had many pores below the tooth surface. The hardness of the tooth surface of mating case-hardened pinion CSCM was *Hv* 800, and the effective hardened depth was 0.8 mm.

Experimental Procedure

Fig. 2 shows a sketch of the gear testing machine and the measuring system for tooth root strain, the vibration acceleration and the sound pressure from the gearbox. The test apparatus used in this experiment was a power circulating type gear testing machine with a center distance of 82.55 mm. This machine was operated by driving a power transmission gear set through a Kopp variable speed drive with an electric motor.

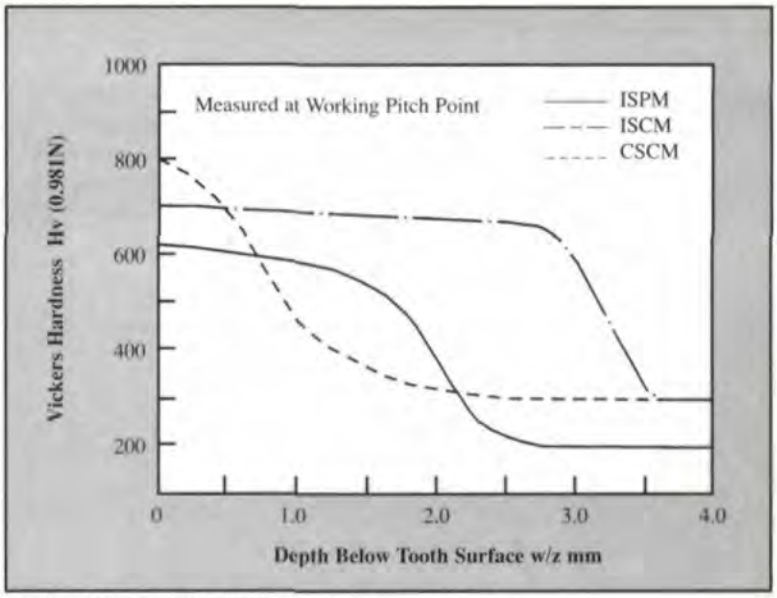

Fig. 1 — Hardness distributions of test gears and pinions.

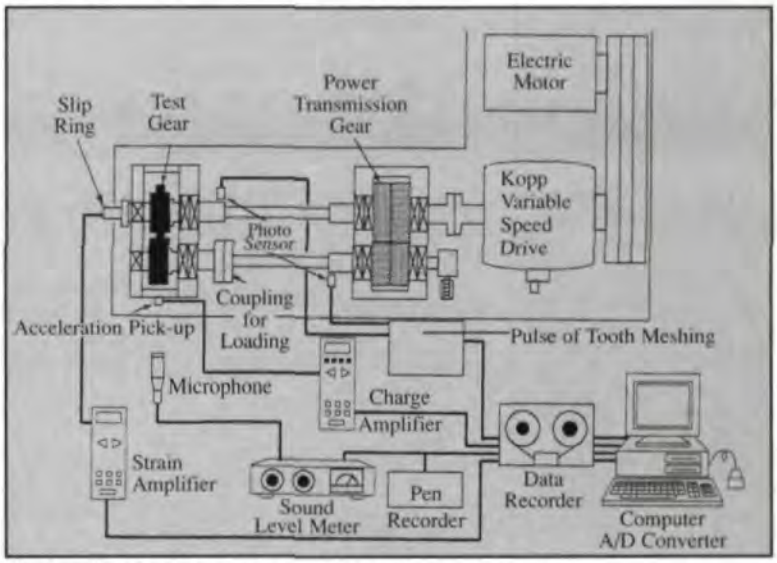

Fig. 2 — Sketch of gear testing machine and measuring system.

The fatigue tests were conducted at a rotation speed n_2 of 1800 rpm for test gears. The lubricant employed here was a gear oil with EP additives that had a kinematic viscosity of 190.9 x 10^{-6} m^2/s at 313 K and a viscosity index of 98. The oil was supplied to the engaging side of a test gear pair at a rate of 750 ml/min. The supplied oil temperature was 313 ± 5 K. The maximum Hertzian stress p_{max} at the working pitch point was taken as a scale for loading in this experiment.

The dynamic tooth root strain was measured using a dynamic strain amplifier and a wire strain gage bonded on a compression side of the tooth fillet. The vibration acceleration of the gearbox was detected by a piezo-electric pickup through an amplifier. The sound pressure was detected by a condenser microphone fixed at a distance of 300 mm from the gearbox. To evaluate the dynamic tooth root stress, the static tooth root strain was measured at a rotation speed of 6.6 rpm for the test gear. The tooth profile measurement

Akira Yoshida
is a professor in the Mechanical Engineering Dept. at Okayama University, Tsushima, Japan.

Yuji Ohue
is a research assistant at the same university.

Isamu Karasuno
is general manager of the Material Evaluation Division of Sumitomo Metal Industries Co., Ltd., Osaka City, Japan.

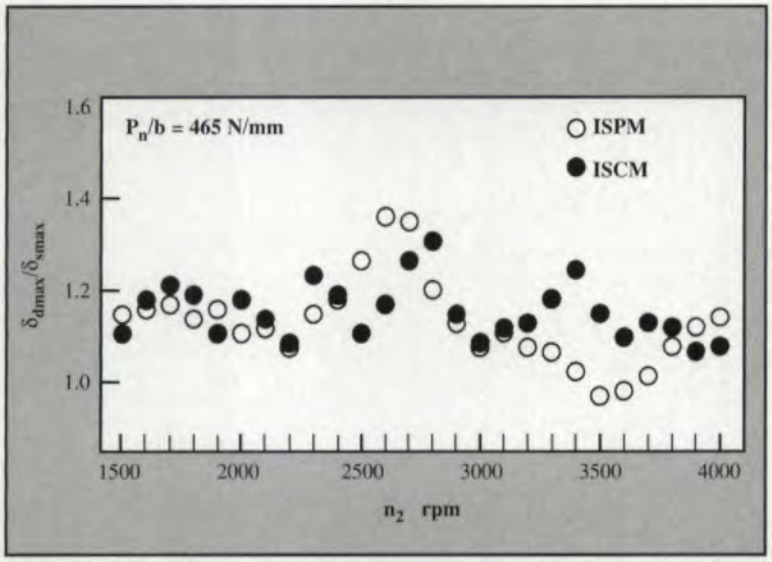

Fig. 3 — Ratio $\delta_{dmax}/\delta_{smax}$ of dynamic maximum tooth root stress to static maximum tooth root stress.

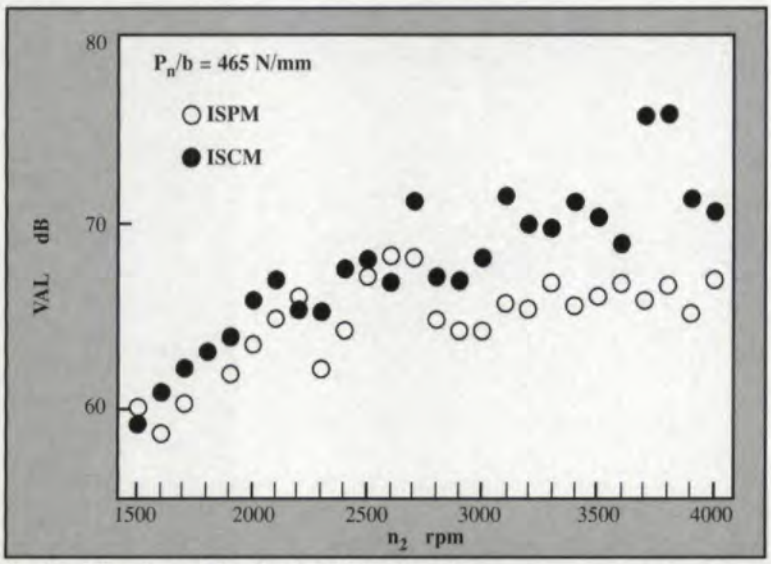

Fig. 4 — Vibration acceleration level *VAL* of gearbox.

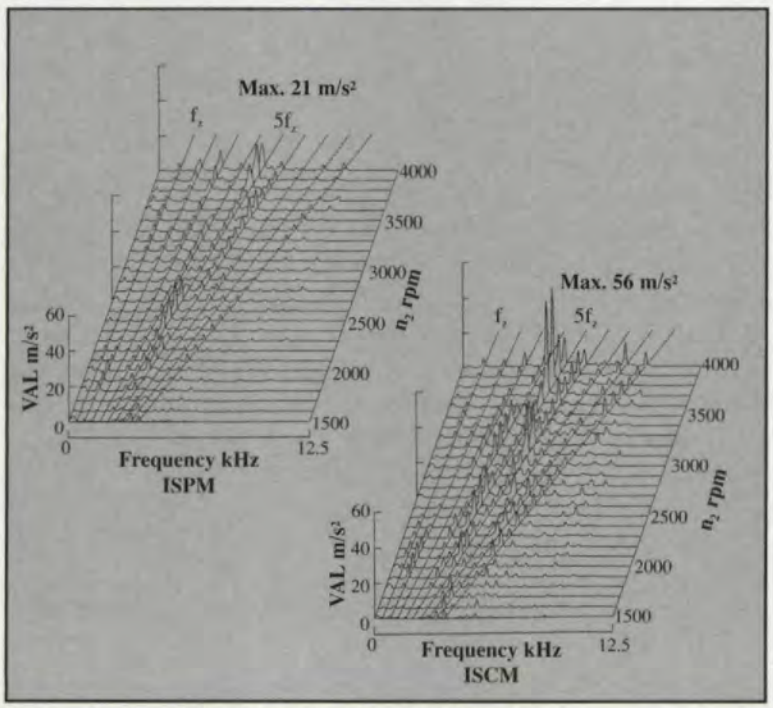

Fig. 5 — Spectra of vibration acceleration of gearbox.

and the replica observation of the tooth surface were also performed. These measurements of the dynamic performance and the observations of the test gear pair were conducted at regular intervals during the fatigue process. A vibration-sensitive shutoff transducer was fixed on the testing machine, stopping the machine automatically when a vibration increase caused by the tooth failure was detected.

Experimental Results and Discussions

Dynamic tooth root stress & vibration acceleration of a gearbox at rotational speeds of 1500–4000 rpm. To compare the dynamic performance of the sintered gear with the steel gear under a normal load per unit face width *Pn/b* of 465 N/mm, the dynamic tooth root stress and the vibration acceleration of both test gears were measured at rotational speeds n_2 of 1500–4000 rpm.

Fig. 3 shows the ratio $\delta_{dmax}/\delta_{smax}$ of the dynamic maximum tooth root stress δ_{dmax} to the static maximum tooth root stress δ_{smax}. The changes of the ratio $\delta_{dmax}/\delta_{smax}$ of both gears ISPM and ISCM were almost the same up to a rotational speed n_2 of 2400 rpm. The ratio $\delta_{dmax}/\delta_{smax}$ of ISPM was lower than that of test gear ISCM at a rotational speed n_2 of more than 300 rpm. In the range of rotational speeds n_2 of 1500–4000 rpm, the ratio $\delta_{dmax}/\delta_{smax}$ for ISPM became the peak value at a rotational speed n_2 of 2600 rpm, while the ratio for ISCM became the peak values at rotational speeds of 2800 and 3400 rpm.

Fig. 4 shows the vibration acceleration level *VAL* of the gearbox. The changes of the value of *VAL* for both ISPM and ISCM were almost the same up to a rotational speed n_2 of 2600 rpm. The values of *VAL* for ISPM were lower than those for ISCM at a rotational speed n_2 of more than 2700 rpm. Especially at rotational speeds n_2 of 3700 and 3800 rpm, the values of *VAL* for ISCM were about 10 dB higher than those for ISPM.

Fig. 5 shows the spectra of the vibration acceleration of the gearbox. For both test gears, the main components of the vibration acceleration of the gearbox were the tooth meshing frequency f_z and its harmonics. The components of a tooth meshing frequency of $5f_z$ at rotational speeds n_2 of 3700 rpm ($5f_z$ = 4.93 kHz) and 3800 rpm ($5f_z$ = 5.07 kHz) were considerably higher than the others. The vibration of the gear pairs caused by tooth meshing at these rotational speeds was resonated with the natural frequency of the gearbox, since the gearbox of the testing machine used in this experiment had a natural frequency of about 5 kHz. The values of spectra at $5f_z$ of test gear ISPM were lower than those of test gear ISCM at a rotational speed n_2 of more than 2700 rpm.

Since the vibration of the gear pair caused by tooth meshing travels to the gearbox through the shafts and bearings supporting the gear, the damping characteristics of gears can be evaluated by the dynamic tooth stress and the vibration of the gearbox. These results show that the damping characteristics of the sintered gear ISPM are slightly better than those of the steel gear ISCM at the rotational speeds n_2 of 1500–4000 rpm in this experiment.

Surface durability and failure mode. Fig. 6 shows the relationship between the maximum Hertzian stress p_{max} at the working pitch point and the number N_2 of cycles to failure. The percentage of the pitted area is defined as a ratio of total pitted areas to total areas of working tooth surfaces on both gear and pinion. In the case of ISPM, the failure mode was pitting with spalling (Ref. 5), and the fatigue life for pitting was taken as a number of cycles of the test gear when a percentage of pitted area reached 5%. The pitted areas also included spalled areas.

In the case of test gear ISCM, the failure mode was tooth breakage caused by pitting near the working pitch point, and the fatigue life was taken as the number of cycles made by the test gear when tooth breakage due to pitting automatically stopped the testing machine. In this case, the tooth breakage caused by pitting occurred before the percentage of pitted area reached 5%. The test gear ISCM, fatigue-tested under a Hertzian stress p_{max} of 1600 MPa, did not fail up to a number N_2 of 10^8 cycles. The surface durability at a number N_2 of 10^8 cycles in ISPM was 870 MPa, and that in ISCM was 1600 MPa.

Fig. 7 shows photographs of whole failed tooth surfaces and magnified photographs on the dedendum tooth surfaces of both test gears at a final fatigue stage. Those photographs were taken by a scanning electron microscope. On the failed tooth of test gear ISPM, which had some large pits, one can observe many small pits. On the dedendum tooth surface, pits having diameters of 10 to 100 μm were observed, while on the failed tooth of ISCM, large pits were observed near the working pitch point. The tooth breakage caused by pitting in test gear ISCM occurred from the bottom of the large pits near the working pitch point. On the dedendum tooth surface, the surface was smooth and a few small pits were observed.

The percentage of the pitted area in ISPM increased progressively, because the number of small pits increased gradually (Ref. 5). Spalling failure was also observed on the tooth surface near the working pitch point during the fatigue process (Ref. 5). On the other hand, the percentage of the pitted area in ISCM increased sharply, because large pits appeared rapidly at the final fatigue stage. Spalling failure was not observed in these fatigue tests. Under a Hertzian stress p_{max} of 1600 MPa, pits were not observed on the tooth surfaces of ISCM up to a number N_2 of 10^8 cycles.

Fig. 8 shows transverse sections near the tooth surface of test gear ISPM before and after the fatigue test. The pores existing below the tooth surface are visible. The mean size of pores in the transverse section is about 15 μm in diameter. In

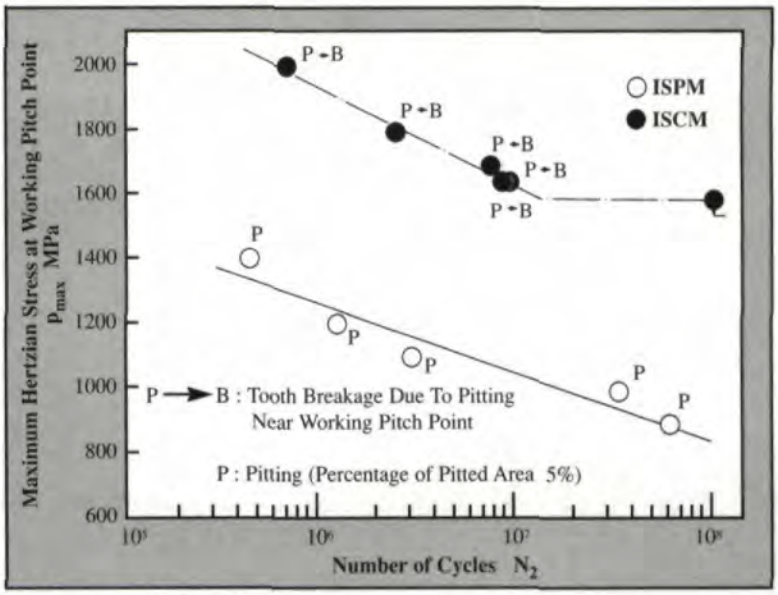

Fig. 6 — p_{max} - N_2 curves.

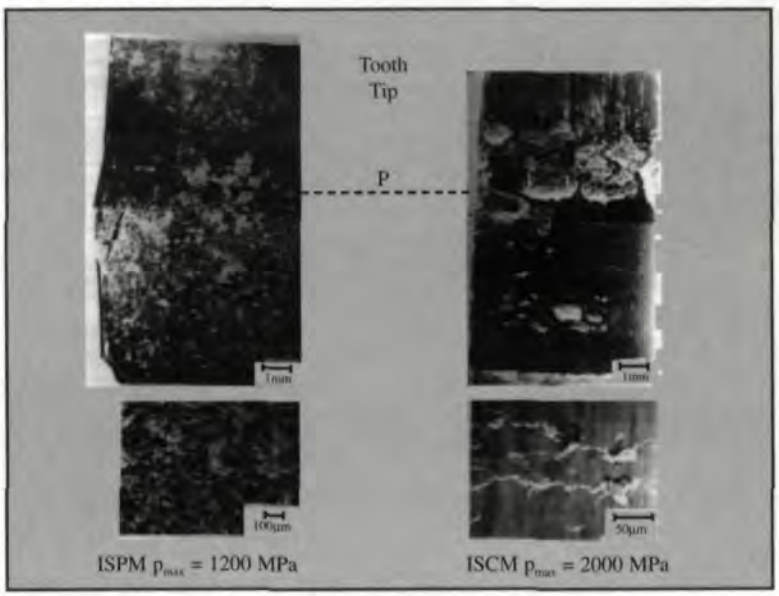

Fig. 7 — Failed tooth surfaces observed by *SEM*.

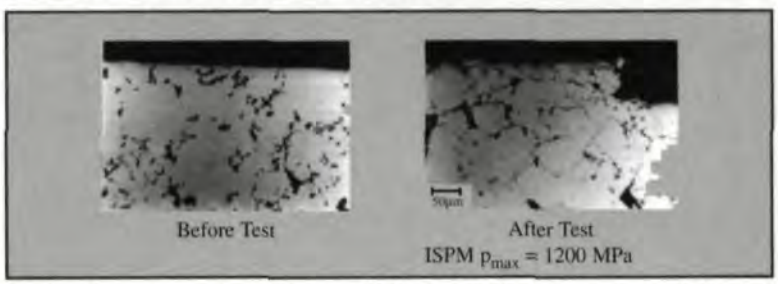

Fig. 8 — Transverse sections of test gear ISPM near tooth surface before and after test.

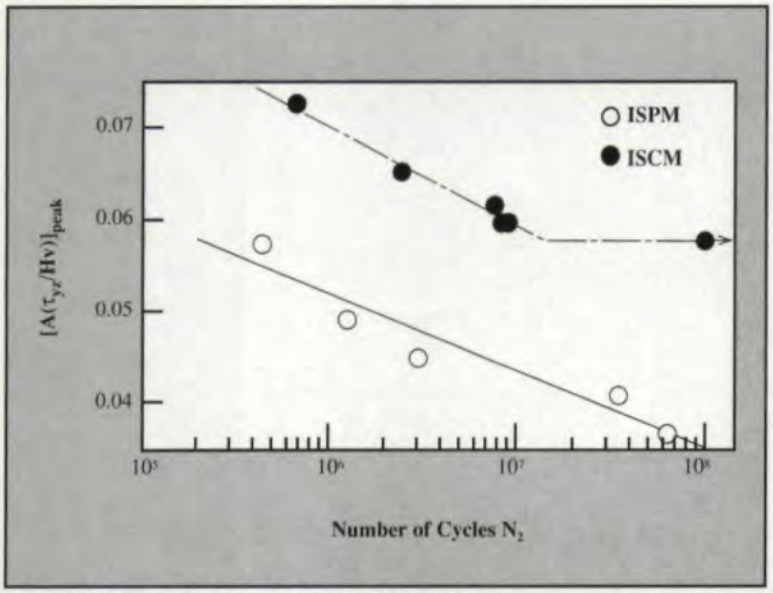

Fig. 9 — Relationships between $[A(\tau_{yz}/Hv)]_{peak}$ and N_2.

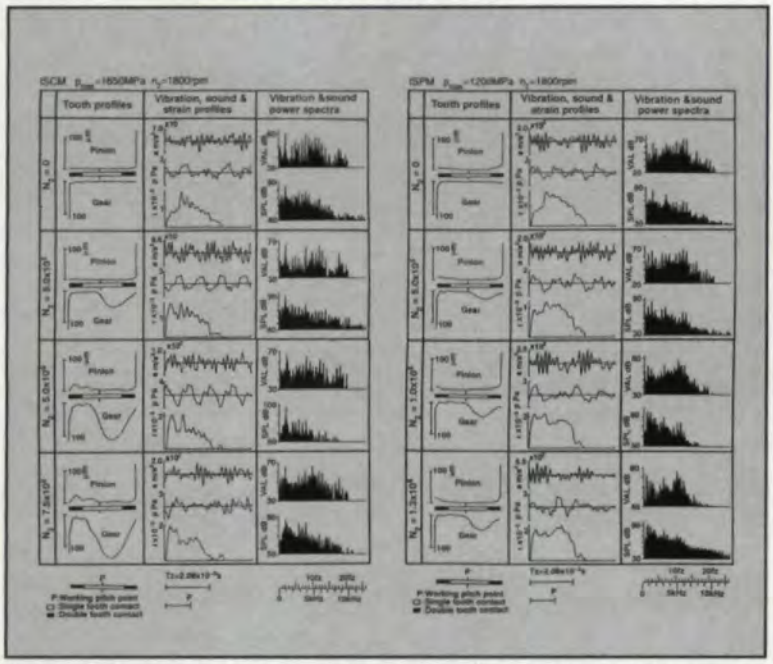

Fig. 10 — Changes in tooth profiles and dynamic performance during fatigue process.

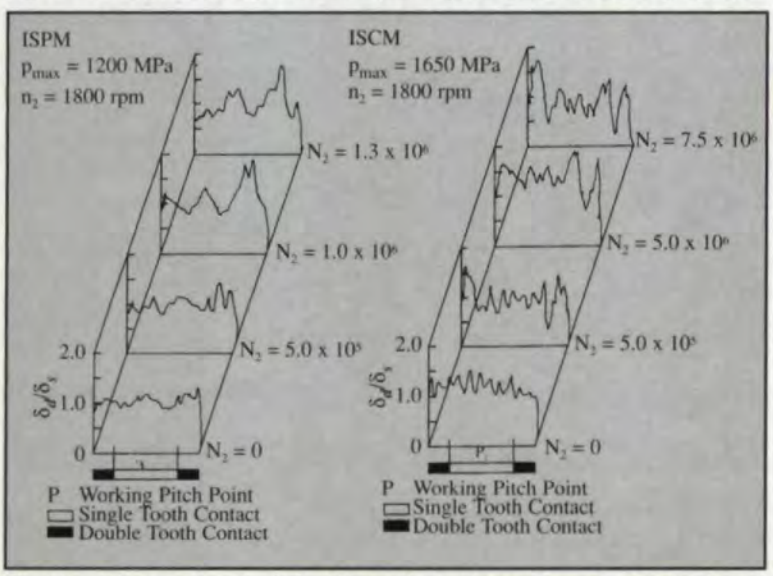

Fig. 11 — Changes in ratio δ_d/δ_s of dynamic tooth root stress to static tooth root stress during fatigue process.

the post-test photograph, the pores are linked to each other by cracks. Therefore, it can be assumed that these cracks caused small pits, and the formation mechanism of pits in sintered gears is different from that in steel gears.

In order to clarify design methods to reduce spalling failure rates in surface-hardened steel rollers and gears, the authors have studied their surface durability using an amplitude of the ratio of orthogonal shear stress to Vickers hardness below the surface (Refs. 8–9). The calculation methods of the spalling fatigue life and the allowable load for spalling were proposed using the amplitude of the ratio of shear stress to hardness (Ref. 8). In this article, the same method was also applied to a sintered gear. Fig. 9 shows the relationship between the peak amplitude $[A(\tau_{yz}/Hv)]_{peak}$ of the ratio of orthogonal shear stress τ_{yz} to Vickers hardness Hv and the number N_2 of cycles. The stresses below the tooth surface at the working pitch point were calculated by an analytical method after Smith and Liu (Ref. 10). It was also assumed here that the material strength of each test gear is directly proportional to each Vickers hardness. In this fatigue test, the spalling failure for test gear ISCM was not observed. But the relationship $[A(\tau_{yz}/Hv)]_{peak}$ - N_2 in test gear ISCM was located lower than that in ISPM because of the porous quality of the sintered gear. This fact indicates that the relationship between the material strength and the hardness in the sintered gear is different from that in the steel gear.

Changes in dynamic performance during fatigue process. Fig. 10 shows an example of the changes in the tooth profiles of gear and pinion, vibration acceleration a, sound pressure p, compressive tooth root strain ε, and vibration and sound spectra during a fatigue process at a rotational speed n_2 of 1800 rpm. Since the Hertzian stress p_{max} for test gear ISPM was different from that for test gear ISCM in Fig. 10, ISPM was qualitatively compared with ISCM on dynamic performance. Concerning the tooth profile change, wear of both ISPM and ISCM occurred on the dedendum tooth surface at an initial fatigue stage and developed in the direction of the working pitch point as the number of cycles increased. The tooth profile of the mating pinions of both test gears did not change remarkably during the fatigue stage. The profiles of vibration acceleration and sound pressure change periodically at tooth meshing period Tz at the initial fatigue stage. As the number of cycles increased, the profiles of both of them changed gradually through the fatigue process. But the profile did not change periodically at the final fatigue stage.

In the results of the spectra analysis, the main components of the spectra of both *VAL* and *SPL* were the tooth meshing frequency f_z and its harmonics at the initial fatigue stage. But the values of the components, except for the tooth meshing frequency and its harmonics, became gradually higher as the number of cycles increased. Comparing the profile change of the tooth root strain near the final fatigue stage with that at the initial fatigue stage, we can see that the load in the test gear was not smoothly transmitted at the recess contact zone. These dynamic performances during the fatigue tests were qualitatively similar in both test gears.

To evaluate the dynamic tooth root stress quantitatively, the dynamic tooth root stress was evaluated by comparing the changes of the ratio δ_d/δ_s of dynamic tooth root stress δ_d to static tooth root stress δ_s at each contact position during the fatigue process. Fig. 11 shows the changes of the ratio δ_d/δ_s during the fatigue process. At the initial fatigue stage, the value of the ratios δ_d/δ_s for each test gear was near 1.0 through tooth meshing. The profile of the ratio for ISPM changed more smoothly through the tooth meshing compared with that for ISCM. This fact indicates that the damping characteristic of ISPM was superior to that of ISCM. As a number of cycles increased, the profile of the ratio for both test gears changed gradually. Especially at the final fatigue stage for both gears, the profile of the ratio at the recess contact zone changed rapidly because of the wear of the tooth surface. In the case of test gear ISCM, the profile of the ratio δ_d/δ_s also fluctuated widely at the beginning of the tooth meshing from the early fatigue stage.

Conclusions

To discover how to apply surface-hardened, sintered, powder metal gear technology to power transmission gears, an induction-hardened, sintered powder metal spur gear was compared with an induction-hardened, melted steel spur gear for surface durability and dynamic performance. The fatigue tests were conducted using a power circulating gear testing machine having a center distance of 82.5 mm. The results are summarized as follows:

1. Under the same normal load per unit face width, the sintered gears were slightly superior to the steel gears on the dynamic tooth stress and the vibration acceleration of the gearbox at rotational speeds of 1500–4000 rpm.

2. The surface durability of the sintered gear was lower than that of the steel gear. The failure mode of the sintered gear was pitting with spalling, while that of the steel gear was tooth breakage due to pitting near working pitch point. The pitted area of the sintered gear increased gradually during the fatigue process. On the other hand, that of the steel gears increased rapidly at the final fatigue stage. The pitting of the sintered gear was mainly caused by the porous nature of the material. The pores existing on and below the tooth surface of the sintered gear played an important role in pit formation.

3. In both cases, the wear of the tooth profile occurred at the dedendum tooth surface because of tip interference between gear and pinion, and was developed in the direction of the working pitch point during the fatigue process. The changes in the dynamic performance of both test gears were almost the same qualitatively during the fatigue process. ○

References:

1. Bertilsson, I. & B. Karlsson. "Dynamic Properties of Sintered Steel." *Powder Metallurgy*, Vol. 30, No. 3, 1987, pp. 183–188.
2. Ledoux, L. & C. Prioul. "Influence of Pore Morphology on the Monotonic and Cyclic Properties of Sintered Iron." *Metallurgy of Powder Report*, Vol. 44, No. 6, 1989, pp. 438–442.
3. Lindqvist, B. "Influence of Microstructure and Porosity on Fatigue Properties of Sintered Steels, *Metallurgy of Powder Report*, Vol. 44, No. 6, 1989, pp. 443–448.
4. Yoshida, A. et al. "A Study on Surface Durability of Induction-Hardened Sintered Powder Metal Rollers." *JSME International Journal*, Series 3, Vol. 34, No. 3, 1991, 419–426.
5. Yoshida, A. et al. "A Study on Fatigue Strength of Induction-Hardened Sintered Powder Metal Gears." *Proceedings of JSME International Conference on Motion & Power Transmissions*, 1991, pp. 757–762.
6. Yoshida, A. et al. "Surface Failure and Durability of Induction-Hardened Sintered Powder Metal Rollers and Gears With Various Hardened Depths." *Proceedings of 1992 International Power Transmission & Gearing Conference*, Vol. 2, 1992, pp. 733–740.
7. Yoshida, A. et al. "Surface Durability of Induction-Hardened Sintered Powder Metal Rollers in Relation to Number and Size of Pores." *Proceedings of the First China/Japan International Symposium on Machine Elements*, Vol. 1, 1993, pp. 49–54.
8. Yoshida, A. et al. "Estimation of Fatigue Strength for Surface Failure of Surface-Hardened Steel Rollers and Gears." *Proceedings of International Conference on Gearing*, Vol. 2, 1988, pp. 515–518.
9. Yoshida, A. et al. "Effect of Standard Pressure Angle on the Fatigue Strength of Nitrided Gears." *JSME International Journal*, Series 3, Vol. 31, No. 1, 1988, pp. 84–91.
10. Smith, I. O. & C. K. Liu. "Stresses Due to Tangential and Normal Loads on an Elastic Solid With Application to Some Contact Stress Problems.," *Transactions of ASME, Journal of Applied Mechanical Engineering*, Vol. 20, No. 2, 1953, pp. 157–166.

Originally presented at the 1994 International Gearing Conference, University of Newcastle upon Tyne, U.K., September, 1994.